Elasto-visco-plastic modeling of mild steels for sheet forming applications over a large range of strain rates

Jean-Marc Pipard [a,b], Tudor Balan [a,*], Farid Abed-Meraim [a], Xavier Lemoine [a,b]

[a] Laboratoire d'Étude des Microstructures et de Mécanique des Matériaux, LEM3, UMR CNRS 7239, Arts et Métiers ParisTech, 4 rue Augustin Fresnel, 57078 Metz Cedex 03, France

[b] ArcelorMittal R&D Global Maizières, Automotive Product, Voie Romaine, BP 30320, 57283 Maizières-Lès-Metz Cedex, France

Abstract

A physically based elasto-visco-plastic constitutive model is presented and compared to experimental results for three different mild steels. The experiments consist of tensile tests ranging from quasi-static conditions up to strain rates of 10^3 s^{-1} as well as quasi-static simple and reverse shear tests at different amounts of pre-strain. Additional two-step sequential mechanical tests (Bauschinger and orthogonal effects) have been performed to further evaluate the ability of the model to describe strain-path changes at moderate/large strains. The model requires significantly fewer material parameters compared to other visco-plasticity models from the literature, while being able to describe some of the main features of the strain-rate sensitivity of mild steels. Accordingly, the parameter identification is simple and intuitive, requiring a relatively small set of experiments. The strain-rate sensitivity modeling is not restricted to a particular hardening law and thus provides a general framework in which advanced hardening equations can be adopted.

Keywords: Constitutive behavior; Visco-plasticity; Microstructure-related parameters; Mild steel; Finite element simulation.

* Corresponding author: Tudor Balan (tudor.balan@ensam.eu) tel: +33.3.87.37.54.60, fax: +33.3.87.37.54.70

1 Introduction

Increasingly, drastic safety and environmental requirements are acting as a driving force for the optimization of materials for structural components (body in white) for automotive applications. The energy absorbing components of the car body are deformed at relatively low strain rates during press forming. Eventually, they may undergo very high strain rates, along different strain paths, during crash events. Consequently, the accurate prediction of formability and crashworthiness requires constitutive models adequate to a large range of strain rates, including strain histories typical of both forming and crash. Structural automotive parts are usually made of steel sheets, known for their strain-rate sensitivity. As a consequence, considerable research efforts have been dedicated to the development of constitutive models for steels that are applicable in a strain-rate range up to 10^3 s^{-1}, which covers the typical press forming and crash conditions. Following the pioneering work of Fields and Bachofen (1957), and the still popular models of Perzyna (1963) or Johnson and Cook (1983), numerous phenomenological models have been proposed to describe the combined effect of strain, strain rate and temperature on the flow stress evolution as revealed by experiments (Khan and Huang, 1992; Zhao and Gary, 1996; Molinari and Ravichandran, 2005). Concurrently, a class of more physically based models was inspired from the physical deformation mechanisms observed at the dislocation scale (Zerilli and Armstrong, 1987; Rusinek and Klepaczko, 2001; Rusinek et al., 2007; Zhang et al., 2009; see also the review by Liang and Khan, 1999) which are able to describe the response of various metals and alloys up to very large strain rates, including explosive loading (Preston et al., 2003). Most of these models are restricted to isotropic hardening; Uenishi and Teodosiu (2004) proposed a physically based elasto-visco-plastic model incorporating advanced kinematic hardening. These models apparently involve a large number of material parameters. However, most of them are physical parameters that can be determined without performing mechanical tests. Consequently, the number of fitting parameters is generally smaller than for phenomenological models.

The constitutive framework adopted in this contribution falls into the latter category of physically motivated models, based on the thermal activation theory of cold plastic deformation in crystalline metals and alloys (Seeger, 1955). Some of its basic physical considerations are briefly recalled here; for a more detailed presentation see, e.g., (Uenishi and Teodosiu, 2003, 2004; Uenishi et al., 2005). The resolved shear stress τ induced by dislocation glide on an active slip system is determined by a combination of a threshold stress τ_0 related to lattice friction and solute contents, a "long-range" stress τ_μ generated by extended obstacles, and an effective stress τ^* required for the dislocation to overcome short-distance obstacles with the help of thermal fluctuations. Under simplifying hypotheses of uniform distribution of identical obstacles and neglecting the possibility of backward jumps (*i.e.,* in the direction opposite to the stress), the slip rate on an active slip system of the crystal can be related to the effective stress by the expression

$$\dot{\gamma} = \rho_m \nu_D b l_F \exp\left(-\frac{\Delta G(\tau^*)}{k_B T}\right), \tag{1}$$

where T is the absolute temperature, ρ_m is the mobile dislocation density, b is the Burgers vector magnitude, ν_D is the Debye frequency, k_B is the Boltzmann constant, and l_F is the average flight distance between two successive obstacles. The dependency of Gibbs'

activation free energy ΔG on the effective resolved shear stress τ^* has been often described using power laws (Kocks et al., 1975), *e.g.*,

$$\Delta G(\tau^*) = \Delta G_0 \left[1 - \left(\frac{\tau^*}{\tau_0 + \tau_\mu} \right)^p \right]^q , \tag{2}$$

where ΔG_0 is the average activation free energy required to overcome a local obstacle without applied stress, and p and q are geometric parameters related to the shape of the obstacles. An alternative approach was considered by Sellars and Tegart (1966) and Wong and Jonas (1968), where a simple linear relationship $\Delta G(\tau^*) = \Delta G_0 - \tau^* V^*$ is used while taking into account the possibility of backward jumps, leading to

$$\dot{\gamma} = \dot{\gamma}_0 \sinh \frac{\tau^* V^*}{k_B T} , \tag{3}$$

where $\dot{\gamma}_0 = \rho_m \nu_D b l_F \exp(-\Delta G_0 / k_B T)$.

The resolved shear stress during plastic glide has been often expressed by the simple linear combination $\tau = \tau_0 + \tau_\mu + \tau^*$, which has proved useful especially for FCC metals. Based on the analysis of deformation mechanisms at the dislocation scale in BCC metals, Rauch (1994) proposed an interaction between these terms in the form

$$\tau = \tau_0 + \frac{\tau^*}{2} + \sqrt{\tau_\mu^2 + \left(\frac{\tau^*}{2} \right)^2} . \tag{4}$$

The starting point for the current work is the one-dimensional model of Allain et al. (2009), which combines Eqs. (1), (3), and (4) in an algebraic model with a strong metallurgical background and has shown a good ability to describe the tensile behavior of a large variety of steels (Allain et al., 2010) over a wide range of strain rates. Here, a three-dimensional incremental extension is proposed, which is suitable for finite element implementation and application to multi-axial loading conditions. The set of equations defining the constitutive model is derived in Section 2. The associated parameters are identified for three mild steels in Section 3 to investigate the accuracy and validity of the model, which is also compared to other recent models from the literature. In Section 4, the model is applied to the finite element simulation of a tensile test, including the early post-necking stage. The last section summarizes the main findings and conclusions.

In the following, vector and tensor variables are denoted by boldface symbols. Components, whenever used, are referred to a Cartesian orthogonal frame. The summation convention over repeated indices of such components is used. Let **A**, **B** denote second-order tensors and **C** a fourth-order tensor; the double-contracted tensor products between such tensors are defined as

$$\mathbf{A}:\mathbf{B} = A_{ij} B_{ij}, \quad (\mathbf{C}:\mathbf{A})_{ij} = C_{ijkl} A_{kl}, \quad \mathbf{A}:\mathbf{C}:\mathbf{B} = A_{ij} C_{ijkl} B_{kl} . \tag{5}$$

The norm of **A** is defined as $\|\mathbf{A}\| = \sqrt{\mathbf{A}:\mathbf{A}}$, and its direction, if **A** is non-zero, as $\mathbf{A}/\|\mathbf{A}\|$. Note that all second- and fourth-order tensors that enter the modeling described hereafter are supposed fully symmetric.

2 Elasto-visco-plastic phenomenological model

In metal forming, the sheet generally undergoes large deformations, and its behavior is described by rate constitutive equations. To achieve frame-invariance of the material response, objective rates must be used. A convenient approach used to ensure material frame-invariance while keeping the constitutive equations simple in form, consists of reformulating these equations in terms of rotation-compensated variables. In the following, the tensor quantities are written in such a convenient rotating frame in which simple material time derivatives can be used in the constitutive equations. The material is initially stress-free (a well-annealed state), undamaged, and homogeneous.

The strain rate tensor $\dot{\boldsymbol{\varepsilon}}$ is decomposed into an elastic part $\dot{\boldsymbol{\varepsilon}}^{e}$ and a visco-plastic part $\dot{\boldsymbol{\varepsilon}}^{vp}$, and the linear hypoelastic response of the material is expressed as

$$\dot{\boldsymbol{\sigma}} = \mathbf{C}:\left(\dot{\boldsymbol{\varepsilon}} - \dot{\boldsymbol{\varepsilon}}^{vp}\right), \tag{6}$$

where $\dot{\boldsymbol{\sigma}}$ is the rate of the Cauchy stress tensor $\boldsymbol{\sigma}$ and $\mathbf{C}$ is the fourth-order elasticity tensor. In the case of isotropic linear elasticity, $\mathbf{C} = 2G\,\mathbf{I}_4'^{s} + K\,\mathbf{I}\otimes\mathbf{I}$, with K and G being the bulk and shear moduli, respectively. **I** is the second-order unit tensor, whose components are the Kronecker deltas, *i.e.,* $\mathrm{I}_{kl} = \delta_{kl}$, while $\mathbf{I}_4'^{s}$ is the fourth-order symmetric deviatoric unit tensor, whose components are $\mathrm{I}_{4ijkl}'^{s} = (1/2)(\delta_{ik}\delta_{jl} + \delta_{il}\delta_{jk}) - (1/3)\delta_{ij}\delta_{kl}$.

The flow rule defines the direction of the visco-plastic strain rate as the gradient of a scalar function of the stress tensor components. The equivalent stress σ_{eq} is classically used for this purpose. Here, the von Mises equivalent stress is adopted for simplicity

$$\sigma_{eq} = \sqrt{\tfrac{3}{2}(\boldsymbol{\sigma}' - \mathbf{X}):(\boldsymbol{\sigma}' - \mathbf{X})}, \tag{7}$$

where $\boldsymbol{\sigma}'$ denotes the deviatoric part of the Cauchy stress tensor and the second-order tensor **X** describes the kinematic hardening. The flow rule can be written as

$$\dot{\boldsymbol{\varepsilon}}^{vp} = \dot{\varepsilon}_{eq}^{vp}\mathbf{V} \quad , \quad \mathbf{V} = \frac{\partial\sigma_{eq}}{\partial\boldsymbol{\sigma}} = \frac{3}{2}\frac{(\boldsymbol{\sigma}' - \mathbf{X})}{\sigma_{eq}}, \tag{8}$$

where $\dot{\varepsilon}_{eq}^{vp}$ is the equivalent visco-plastic strain rate. Obviously, any other (anisotropic) yield function can be used in Eqs. (7)-(8) without restriction.

A scalar "overstress" describing the increase of stress intensity due to the visco-plastic strain rate is defined by the following relationship, after (Allain et al., 2009)

$$\sigma^* = K^* \sinh^{-1}\left(\frac{\dot{\varepsilon}_{eq}^{vp}}{\dot{\varepsilon}^*}\right), \tag{9}$$

where K^* and $\dot{\varepsilon}^*$ are material parameters. The strain-rate sensitivity affects both the initial yield stress and the (isotropic) hardening term; in the current model, the previously defined overstress is split in two equal contributions, according to Rauch (1994):

$$\sigma_{eq} - \left(\sigma_0 + \frac{\sigma^*}{2}\right) - \sqrt{R^2 + \left(\frac{\sigma^*}{2}\right)^2} \leq 0, \tag{10}$$

where the strict inequality situation corresponds to elastic loading or unloading. In this equation, σ_0 is a material parameter designating the initial yield stress in quasi-static loading conditions, and R describes the isotropic work-hardening of the material. Notably, any isotropic hardening model can be adopted in this framework. For example, Voce's saturating law

$$\dot{R} = C_R (R_{sat} - R)\dot{\varepsilon}_{eq}^{vp}, \tag{11}$$

where C_R and R_{sat} are material parameters, can be used, as well as Swift's power law

$$\dot{R} = nK^{\frac{1}{n}}\left(K\varepsilon_0^n + R\right)^{\frac{n-1}{n}} \dot{\varepsilon}_{eq}^{vp}, \tag{12}$$

where K, n, ε_0 are material parameters. In Section 4, a six-parameter law will be used, which combines the Voce and the Swift hardening laws

$$\dot{R} = \alpha \dot{R}^V + (1-\alpha)\dot{R}^S, \tag{13}$$

where α is a weighting parameter and the superscripts "V" and "S" designate the "Voce" and "Swift" components, respectively, as defined by Eqs. (11) and (12).

For the sake of simplicity, the kinematic hardening described by the backstress tensor $\mathbf{X}$ is governed by the non-linear model of Armstrong and Frederick

$$\dot{\mathbf{X}} = C_X (X_{sat}\mathbf{N} - \mathbf{X})\dot{\varepsilon}_{eq}^{vp} \quad , \quad \mathbf{N} = \frac{\mathbf{V}}{\|\mathbf{V}\|}, \tag{14}$$

where C_X and X_{sat} are material parameters and $\mathbf{N}$ is the unit vector parallel to the visco-plastic flow direction. It is noteworthy that different evolution laws can be adopted for the backstress tensor, without particular restrictions.

The proposed constitutive model is designed mainly for cold sheet metal forming; however, temperature variations due to plastic deformation may have a non-negligible influence on the current stresses and more specifically on their rate sensitivity. Experimental observations and

modeling justifications based on thermal activation theory, reviewed in the Introduction, allow for straightforward model enrichment to take into account moderate temperature effects. Considering Eq. (3), a classical and straightforward extension of Eq. (9) to include temperature can be written as

$$K^* = K_0^* \frac{T}{T_0} \quad ; \quad \dot{\varepsilon}^* = \dot{\varepsilon}_0^* e^{-\beta \frac{T_0}{T}} , \tag{15}$$

where T is the absolute temperature, T_0 is an arbitrary reference temperature taken equal to 293 K, and K_0^* and β are material parameters compensating for the loss of physical meaning after the simplified scale transition. The constant $\dot{\varepsilon}_0^* \approx 2M\rho_m \nu_D b^2$ (Allain et al., 2009) can be taken equal to 3.75×10^4 s^{-1} based on Eq. (1) and the physical constant values in Table 1. Thus, the temperature sensitivity is included with only two fitting parameters. In addition, the initial yield stress in quasi-static conditions has been shown experimentally to depend on temperature (Uenishi and Teodosiu, 2003). Over the relatively small range of temperatures encountered in cold sheet forming or crash events, a linear variation can be considered

$$\sigma_0(T) = \sigma_0(T_0) + K^T (T - T_0) , \tag{16}$$

where the value of K^T was identified as –0.68 MPa/K by (Allain et al., 2009) based on the experimental data from (Uenishi and Teodosiu, 2003).

Table 1. Approximate values of some physical quantities entering Eq. (3) in the case of steels; M is the so-called Taylor coefficient.

M	ν_D [s^{-1}]	b [m]	k_B [JK^{-1}]	ρ_m [m^{-2}]
3	10^{13}	2.5×10^{-10}	1.38×10^{-23}	10^{10}

When generalizing dislocation-scale models to the continuum scale, the macroscopic (*e.g.*, tensile) stress should be related to the resolved shear stress acting in each grain and on each slip system, whereas the tensile strain rate is determined by volume averaging the contributions of all slip systems in all grains. Such averaging rules can be effectively achieved for a given texture using micro-macro transition schemes (Molinari et al., 1987; Pilvin, 1990; Sabar et al., 2002). An alternative approach was adopted here that is typical of the internal variable formalism: the equations governing the thermally activated plastic slip were formally transcribed at the macroscopic scale by simply replacing the shear rate / stress by the tensile equivalent strain rate / flow stress, respectively. The phenomenological variables and parameters introduced in this way can be supposed to inherit some of the physical significance of their microscopic counterparts, although they cannot be quantitatively related to them. In the next section, these assumptions are confronted to a series of experimental results.

3 Applications and experimental validations

In this work, the model derived in Section 2 has been applied to three ferritic steel sheets: two cold-rolled DC-type sheet steels, and a hot-rolled sheet steel. The sheet thickness was 0.8 mm for the DC05 steel, 1 mm for the DC06 steel and 3 mm for the hot-rolled DD14 steel. The chemical composition of the materials is shown in Table 2. The materials were subjected to tensile tests at different strain rates. Additionally, quasi-static monotonic and reverse shear tests were performed for some of the sheet steels to quantify the kinematic hardening.

The tensile tests at very low strain rate were performed on a conventional screw-driven tension-compression testing machine, following the ISO 6892-1:2009 standard. The length of the uniform zone of the sample was 80 mm for a sample width of 20 mm. The tensile tests at 1 s^{-1} were performed on a 100-kN rapid hydraulic testing machine. The sample width was 13 mm for all of the tests on this machine for a length of the uniform zone of 100 mm. The tensile load is measured by the machine's load cell, while the tensile strain is determined from the measurement of the grip displacement by means of a laser actuator (see also (Berbenni et al., 2004; Durrenberger et al., 2011)). Strain gages were used with split Hopkinson bars to attain the strain rate of 333 s^{-1}. The samples, with 10-mm uniform length and 4-mm width, were bond in the slits of miniature custom grips using polymer glue (see e.g. (Tarigopula et al., 2008) for a recent illustration of the method). The grips had the same diameter as the Hopkinson bars and were screwed directly to their extremities. The experimental tests were performed by the material testing laboratory at ArcelorMittal Research. The experimental load–displacement curves were trimmed at the maximum load point and converted into true stress – true strain values using the sample geometry and the assumption of uniform deformation. All of the tests were duplicated to verify the repeatability. All of the tests were performed at room temperature; the strain and temperature distributions were not measured during the tests.[1]

Table 2. Chemical composition (in 10^{-3} weight %) of the three sheet steels used for the comparison to experiments.

Steels	C	Mn	P	S	N	Al	Ti	Nb	Si	Cu	Cr	Ni	Zr
DC05	8.6	124	6	9	3.9	44	126	<1	8	16	24	20	<1
DC06	1.0	101	7	5	3.6	50	86	-	9	16	24	20	-
DD14	68	293	14	9	3.2	21	18	-	8	6	-	3	-

[1] Note that these experiments only served to illustrate the feasibility of the parameter identification for the proposed model. Accurate experimental results from literature were used instead, in Section 3.4, for the validation of the model.

3.1 Parameter identification procedure

For the parameter identification of the model, the following mechanical tests were used:

- Tensile tests at strain rates of 10^{-2} s^{-1} and 333 s^{-1}.
- Quasi-static reverse shear tests with three amounts of pre-strain: 5%, 10%, and 15% of shear strain, followed by the same amount of reverse shear strain.

For the hardening description, the Voce isotropic hardening law (11) is used along with the Armstrong–Frederick kinematic hardening law (14). Material parameters have been identified through several successive steps. First, the two kinematic hardening parameters (X_{sat} and C_X) were estimated based on chemical composition and average grain size (Bouaziz and Dirras, 2006); the reverse shear tests mainly served for validation. The quasi-static initial yield stress and the two remaining (isotropic) hardening parameters were identified based on the monotonic tensile test in the transverse direction at the lowest strain rate. Finally, the two strain-rate sensitivity parameters (K^* and $\dot{\varepsilon}^*$) were determined using two tensile tests, performed at the two extreme strain rates available. This identification procedure was applied for the DC05 and DC06 sheets. Eventually, for the DD14 sheet the kinematic hardening was neglected and the combined Swift–Voce model in Eq. (13) was used, in view of an application to larger strains. The identified values for the material parameters are provided in Table 3.

Figure 1 compares the predictions of the proposed constitutive model with tensile experiments at two strain rates in the range typical for sheet forming processes, and quasi-static reverse shear tests with three different pre-strain levels, for the DC05 sheet. Figure 2 provides a different representation of the strain-rate sensitivity of this material, emphasizing two regimes often designated as the athermal / thermally activated domains (Campbell and Ferguson, 1970). The increase in the flow stress is accelerated at strain rates larger than 1 s^{-1}, and this trend is described by the model due to the nature of the hyperbolic sinus function. Also, the decrease in the hardening rate emphasized in this figure is predicted in an average manner. As expected, the experimental values corresponding to the extreme strain rates are well predicted, because these values served for the parameter identification. The figures illustrate the capability of the model in predicting the strain-rate sensitivity of ferritic steels over this range of strain rates.

In summary, the proposed model required few experiments for its parameter identification and was able to describe some important trends of the strain-rate sensitivity of this mild steel: the increase of the flow stress with strain rate, its two athermal / thermal regimes, a continuous decrease of the hardening rate.

In the current investigation, the material's anisotropy was neglected. Cold rolled mild steels are anisotropic and the tested DC05 sheet steel had a Lankford coefficient close to 2. In view of the model application to sheet metal forming operations, the plastic anisotropy should be estimated, *e.g.*, by measuring the Lankford coefficients in three in-plane directions. For the current investigation, which was focused on the modeling of strain-rate sensitivity, all of the tests were performed in the transverse direction (*i.e.*, the in-plane material direction perpendicular to the rolling direction). The proposed model can be coupled with any phenomenological yield function to incorporate the description of plastic anisotropy.

Table 3. Material parameters for the three mild steel sheets.

Steels	σ_0 [MPa]	C_R	R_{sat} [MPa]	C_X	X_{sat} [MPa]	K [MPa]	ε_0	n	α	K^* [MPa]	$\dot{\varepsilon}^*$ [s^{-1}]
DC05	155	13	200	100	13	-	-	-	1	36	0.3
DC06	120	8	255	100	13	-	-	-	1	36	0.3
DD14	259	12	147	-	-	543	0.02	0.193	0.1	56.92	0.3

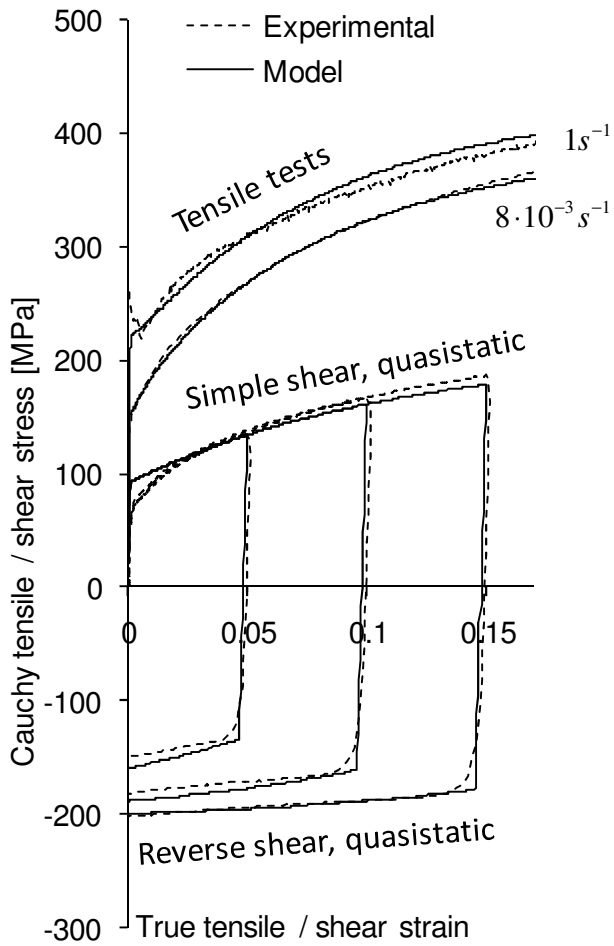

Figure 1. Comparison between experiments (dashed lines) and model predictions (solid lines) for the DC05 steel sheet: monotonic tensile tests (strain-rate sensitivity effect) and quasi-static reverse shear tests after 5%, 10%, and 15% forward shear strain (Bauschinger effect). The abscissa strains are true strains for the tensile tests and amounts of shear strain for the shear tests.

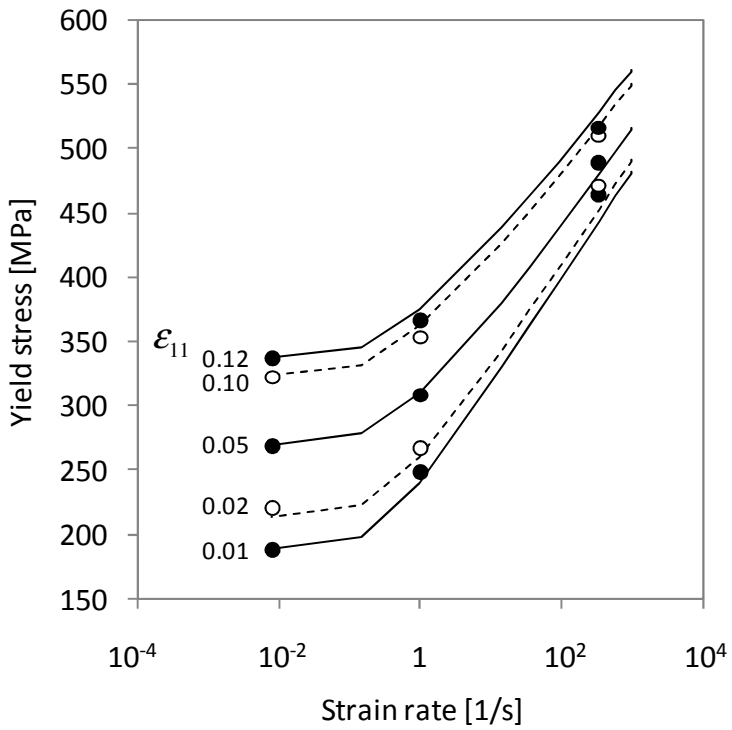

Figure 2. Experimental (symbols) and predicted (lines) flow stresses for the DC05 steel sheet at five levels of cumulated strain for three strain-rate levels.

3.2 Description of temperature effects

As already stated, the temperature evolution during the tensile tests was neglected and it was not taken into account in the simulations. However, the model extension to temperature effects (Eqs. (15)-(16)) has been investigated by performing tensile tests at several temperatures using a thermal chamber on the custom-made rapid hydraulic testing machine. Figure 3 compares the simulation results of the proposed model with experiments for the same DC05 sheet steel at three different values of temperature (–40°C, 20°C and 100°C). The comparison illustrates the ability of the resulting thermo-visco-plastic model to describe the temperature sensitivity of the mean flow stress.

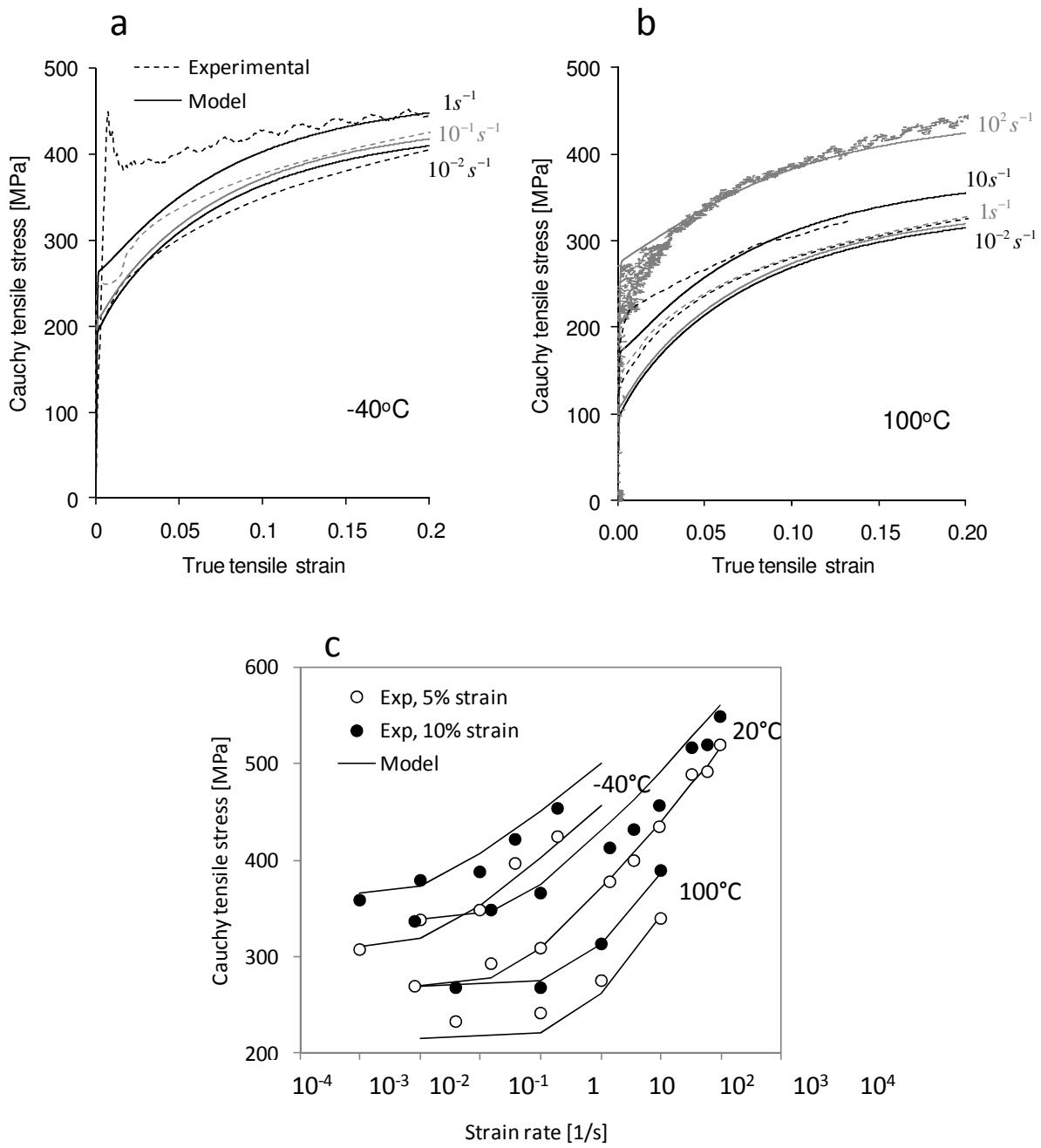

Figure 3. Modeling of the sensitivity of the flow stress to temperature for the DC05 mild steel. Material parameters: $K_0^* = 36$ MPa and $\beta = 11.74$. a) Tensile stress–strain curves at –40°C; b) tensile stress–strain curves at 100°C; c) flow stress as a function of strain rate for the three temperatures.

3.3 Response for two-step sequential loading

To further investigate the ability of the model to describe the strain-path change behavior, large strain two-step sequential tests were performed on the 1-mm-thick DC06 sheet. Quasi-static tensile, shear and reverse shear tests at three levels of pre-strain were performed as well as a shear test following a tensile test in the same direction (orthogonal strain-path change). The same hardening laws are used along with the same parameter identification procedure. The values of the identified material parameters are reported in Table 3, and the predicted stress–strain curves are compared to the experiments in Figure 4. The classical hardening model adopted in these simulations proves to be efficient in describing the hardening behavior of mild steels up to large cumulated strains, including the Bauschinger effect. However, the complex transient response after abrupt strain-path changes cannot be captured with this simple hardening model. Whenever an accurate description of these behavior features is important, *e.g.*, for springback estimation (Haddag et al., 2007), more advanced hardening models should be considered. To this end, several candidate models have been proposed in the literature (Teodosiu and Hu, 1995; Yoshida and Uemori, 2002; Geng et al., 2002; Barlat et al., 2011). Although this type of extension was beyond the scope of the current investigation, it is important to note that such more elaborate hardening equations can be coupled with the proposed model without restriction by replacing Eqs. (11) and (14) with their corresponding counterparts. Along with the reduced number of strain-rate sensitivity parameters, this generality is one of the strengths of the proposed model.

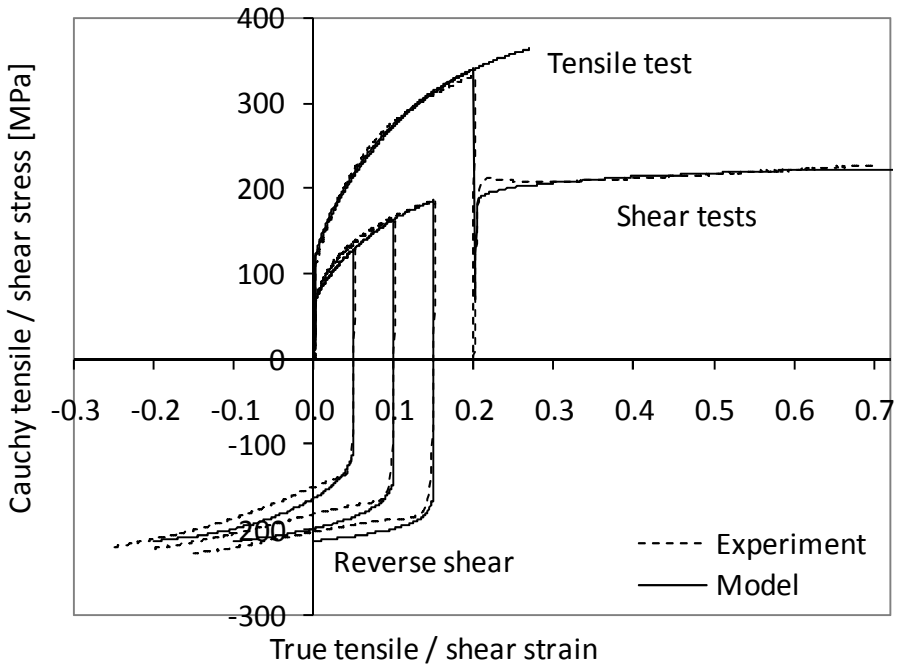

Figure 4. Large strain stress–strain response for the DC06 steel sheet: reverse shear tests after three levels of simple shear pre-strain (Bauschinger tests); shear test following a 20% tensile pre-strain in the same direction (orthogonal test).

3.4 Comparison with other recent visco-plasticity models

In this section, the proposed model is compared with two recent physically motivated phenomenological models from the literature (Uenishi and Teodosiu, 2004; Rusinek and Klepaczko, 2001); these two models will be referred to in the following as U–T and R–K, respectively. These state-of-the-art models have already been compared by their respective authors to more classical constitutive laws (Johnson and Cook, 1983; Cowper and Symonds, 1952). In addition, careful experimental results are available for the parameter identification and model validation.

For the Uenishi–Teodosiu (U–T) model, the yield condition can be formally written as

$$\sigma_{eq} - \left(\sigma_0 + \sigma^*\right) - R - R' \leq 0 \tag{17}$$

where the hardening variable R is described by Voce's law (11) while R' and the kinematic hardening variable $\mathbf{X}$ both depend on two more tensor variables describing the directional strength and the polarity of the persistent planar dislocation structures. The complete description of this advanced hardening model can be found in (Teodosiu and Hu, 1995; Teodosiu, 1997; Haddadi et al., 2006). However, the strain-rate sensitivity (which is of interest for the comparison with the proposed model) only affects σ^* and the saturation value R_{sat} of R by means of the following logarithmic and power laws

$$\sigma^* = \sigma_0^* \left(1 - \frac{T}{F_0} \ln \frac{\dot{\varepsilon}_0^*}{\dot{\varepsilon}_{eq}^{vp}}\right)^2 \;;\; R_{sat} = R_{sat,0} \left(\frac{\dot{\varepsilon}_{eq}^{vp}}{\dot{\varepsilon}_0}\right)^{\nu}. \tag{18}$$

Constants σ_0 and $R_{sat,0}$ are two of the 13 parameters of the Teodosiu–Hu hardening law (Teodosiu and Hu, 1995), while the modeling of strain-rate sensitivity involves four additional fitting parameters: σ_0^*, F_0, $\dot{\varepsilon}_0^*$, and ν [2]. The identification of all of these parameters required the following set of mechanical tests (Uenishi and Teodosiu, 2004): uniaxial tensile tests at different strain rates (10^{-2} and 10^3 s^{-1}), monotonic simple shear tests, reverse shear tests, simple shear following uniaxial tensile tests in the same direction (orthogonal strain-path change), and strain-rate jump tests in tension from 10^{-2} s^{-1} to 10^3 s^{-1}. The experimental results are represented in Figure 5 (dashed lines) along with the predictions of the U–T model (gray lines) based on (Uenishi and Teodosiu, 2004). The proposed constitutive model has been adjusted for this material using the monotonic shear and tensile tests at two strain rates shown in Figure 5. Voce's isotropic hardening and the kinematic hardening Eq. (14) were used; the kinematic hardening parameters were identified based on the chemical composition and grain size. The resulting parameters are summarized in Table 4, and the predictions of the proposed model are shown in Figure 5. Inspection of the figure shows that all of the monotonic tests, at different strain rates, are described satisfactorily and that the Bauschinger effect is well captured in an average manner, as previously shown in Figure 1. As anticipated, the Teodosiu–Hu hardening model accurately describes the complex transient behavior after abrupt strain-path changes and could thus be a good candidate to further enhance the current model in terms of hardening. Leaving apart the effect of this

[2] Uenishi and Teodosiu (2004) consider $\dot{\varepsilon}_0$ as a reference strain rate, set to 10^{-3} s^{-1}, not as a fitting parameter.

difference in the hardening models, Figure 5 reveals that the strain-rate sensitivity description provided by the two models is equally successful in describing the experiments.

Table 4. Material parameters used for the comparison with the U–T and R–K models.

σ_0 [MPa]	C_R	R_{sat} [MPa]	C_X	X_{sat} [MPa]	K [MPa]	ε_0	n	α	K^* [MPa]	$\dot{\varepsilon}^*$ [s^{-1}]
115	8	255	100	13	-	-	-	1	27.2	0.046

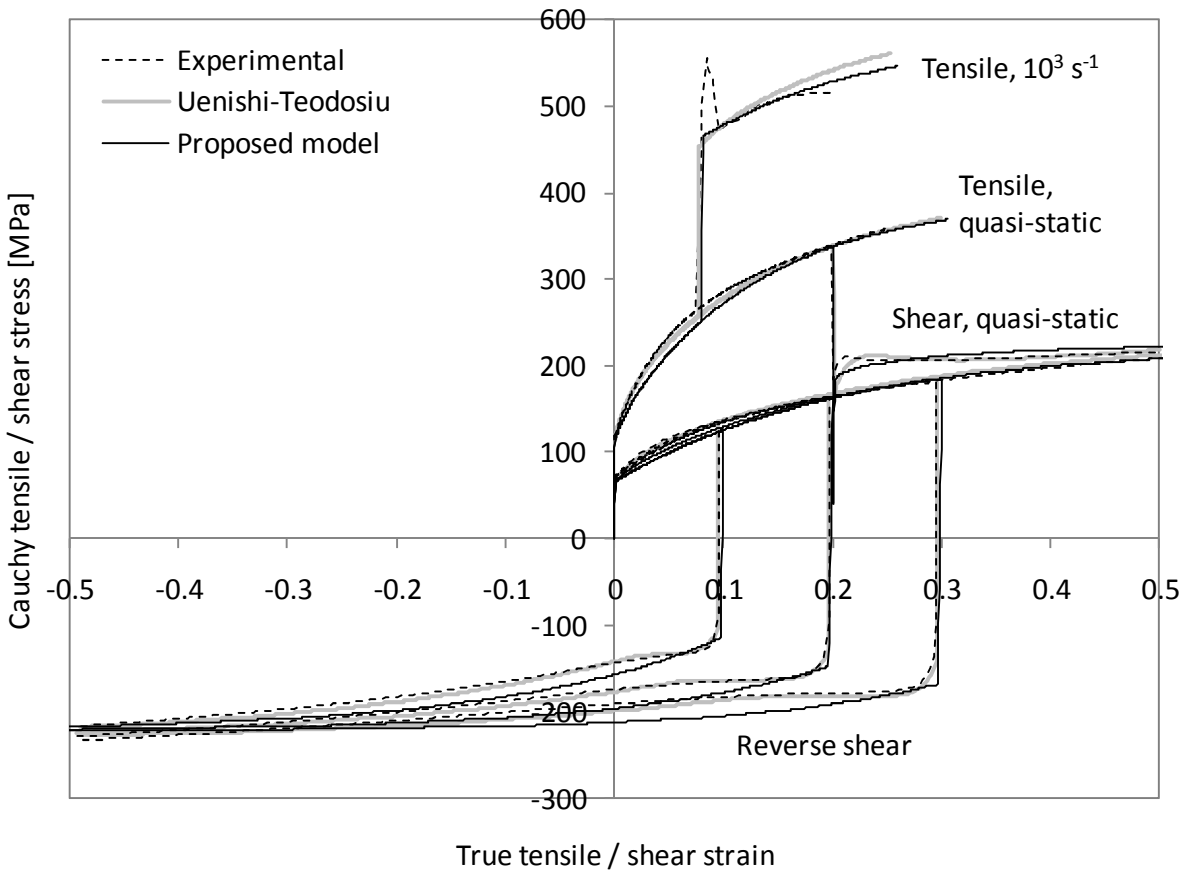

Figure 5. Comparison of the proposed model with the Uenishi–Teodosiu model and experiments, after (Uenishi and Teodosiu, 2004).

The elasto-visco-plastic model proposed by Rusinek et al. (2007) instead uses the Swift hardening law

$$\sigma_{eq} - \sigma^* - K\left(\varepsilon_0 + \varepsilon_{eq}^{vp}\right)^n \leq 0 \tag{19}$$

and a different combination of power and logarithmic laws to describe the strain-rate sensitivity of σ^*, K, and (most importantly) n:

$$\sigma^* = \sigma_0^*\left(1 - D_1 \frac{T}{T_m}\log\frac{\dot{\varepsilon}_{max}}{\dot{\varepsilon}_{eq}^{vp}}\right)^{\frac{1}{m}} \;;\; K = K_0\left(\frac{T}{T_m}\log\frac{\dot{\varepsilon}_{max}}{\dot{\varepsilon}_{eq}^{vp}}\right)^{-\nu} \;;\; n = n_0\left(1 - D_2 \frac{T}{T_m}\log\frac{\dot{\varepsilon}_{eq}^{vp}}{\dot{\varepsilon}_{min}}\right). \tag{20}$$

In the current comparison, the temperature effect is neglected, and thus, the temperature T is considered as a constant. Besides some physical parameters such as the melting temperature T_m, the Rusinek–Klepaczko (R–K) model involves several parameters that require identification. Three parameters enter the hardening law (K_0, n_0, and ε_0), while the strain-rate sensitivity is described using seven additional parameters: σ_0^*, m, ν, D_1, D_2, $\dot{\varepsilon}_{min}$, and $\dot{\varepsilon}_{max}$. The R–K model predictions for a mild steel sheet are reproduced in Figure 6 based on (Rusinek et al., 2007). Because no kinematic hardening is considered in the R–K model, only monotonic tests are shown at different strain rates. According to Figure 6, the predictions of the proposed model offer an equivalent description of the material response both in terms of hardening and strain-rate sensitivity. The parameters from Table 4 were used, because the experimental results in the two references correspond to the same material.

In conclusion, the proposed model proved similar abilities to describe the strain-rate sensitivity of mild steels in the range of strain rates up to 10^3 s^{-1}, compared to the U–T and R–K models, with respect to the experiments exhibited in Figures 5 and 6. More discriminating experiments would be necessary to further differentiate the three approaches.

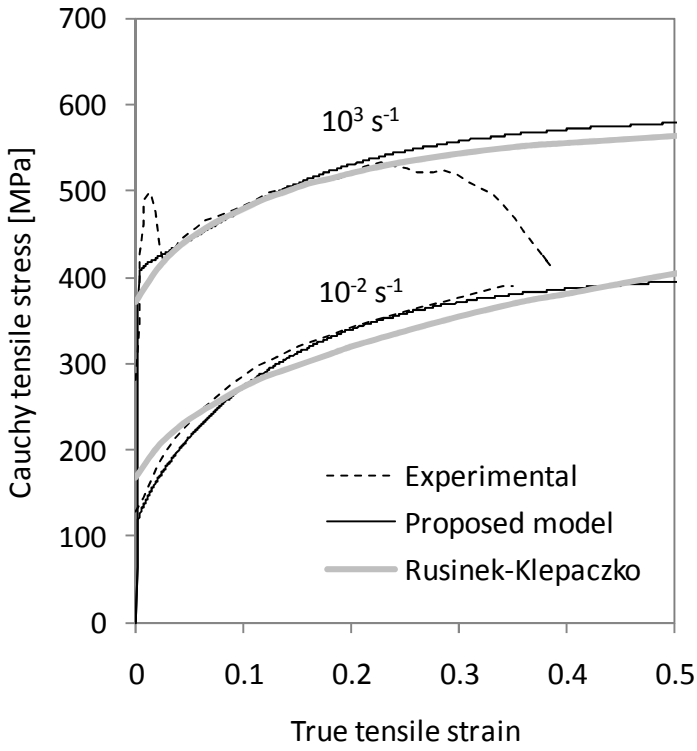

Figure 6. Comparison of the proposed model with the Rusinek–Klepaczko model and experiments, after (Rusinek et al., 2007).

4 Simulation of post-necking tensile response

The constitutive model was implemented in the commercial finite element code Abaqus/Explicit using an explicit time-integration scheme (Haddad et al., 2003; Pipard, 2012) to allow for the simulation of sheet metal forming and crash experiments. Visco-plastic modeling up to large strain rates is a prerequisite for the simulation of high-speed deformation events such as crash; however, this is also required for the accurate simulation of common sheet metal forming processes, *e.g.*, as soon as necking phenomena take place. This well-known statement is illustrated here by the finite element simulation of a simple tensile test. Four simulations are compared, where the only differences concern the constitutive models:

- A strain-rate insensitive model using the isotropic hardening law of Voce – this model will be called "Voce quasi-static" in the following;
- A strain-rate insensitive model using an isotropic hardening model combining the Swift and Voce laws, called "S–V quasi-static";
- The proposed elasto-visco-plastic model, using the same hardening equations and parameters as the "Voce quasi-static" model, called "Voce visco-plastic";
- The proposed elasto-visco-plastic model, using the same hardening equations and parameters as the "S–V quasi-static" model, called "S–V visco-plastic".

At large plastic strains, the selection of an appropriate hardening model is a key factor for accurate finite element simulations. Lemoine and co-workers (Lemoine, 2007; Bui-Van et al., 2009; Lemoine et al., 2011) pragmatically addressed this issue by comparing several classical isotropic hardening models, namely the saturating Voce model, the Swift power law, the Hollomon law, the Ludwig law and the S–V model. The model parameters were identified with respect to standard tensile tests, and they were further confronted to experiments that allowed much larger plastic strain levels (*i.e.*, uniaxial tensile test with local strain measurement, simple shear test, hydraulic bulge test, stack compression test, uniaxial tensile test after flat rolling pre-strain). These studies emphasized the ability of the S–V model to approach the actual material response at large strains, with respect to the other investigated models. These conclusions were confirmed on a wide range of steel grades. Sung et al. (2010) investigated several high-strength (HS) sheet steels, further including strain-rate and thermal effects, and independently emphasized the good performance of a similar Hollomon–Voce linear combination to describe the material response at strains beyond the fit range. These investigations have also shown that the issue of stress–strain curve extrapolation at large strains is more critical for HS steels than for mild steels (see also the discussion by Mohr and Ebnoether (2009)), due to the much smaller range of uniform elongation allowed by HS steels. Because the current study concerns mild steels, the above results have motivated the choice of the combined S–V isotropic hardening model for the application to the flat specimen under uniaxial tension including the post-necking regime. Kinematic hardening was neglected in this analysis because the loading history is monotonic and the focus is on the effect of strain-rate sensitivity. A 3-mm-thick, hot rolled, almost isotropic[3] DD14 mild steel sheet was used for the experiments. The parameters for this material using the Swift–Voce hardening law were previously given in Table 3. Figure 7 shows that the theoretical tensile predictions of the four models (at a uniform deformation and very low strain rate) are similar in the strain range of the uniaxial tensile test, but differences are visible at larger strains.

[3] The values of the Lankford coefficients measured for this sheet steel in the rolling, transverse and diagonal directions, were r_0=1.0, r_{90}=1.1, r_{45}=1.35.

Because the results in Figure 7 are obtained in quasi-static conditions of homogeneous deformation, the responses of the proposed visco-plastic model using Voce and Swift–Voce (S–V) hardening laws, respectively, coincide with those of their strain-rate insensitive counterparts.

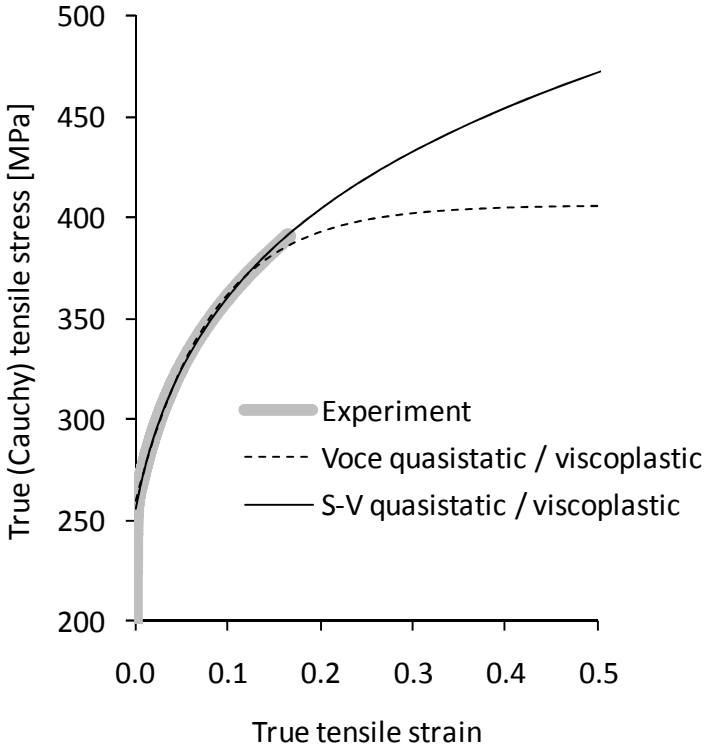

Figure 7. Theoretical tensile material response of the DD14 steel sheet in quasi-static conditions and isotropic hardening model predictions.

The sample geometry and finite element mesh used for the numerical simulation of the tensile tests are shown in Figure 8. One quarter of the sample is meshed using linear reduced-integration hexahedra (C3D8R). The engineering stress–strain predictions corresponding to the four simulations are compared to the experimental results in Figure 9 (left). As expected, Voce's hardening model with the selected parameters predicts earlier necking instability than the Swift–Voce law due to its saturating behavior and smaller hardening rate. While the predictions of the rate-dependent and rate-independent models overlap at small strain rates, their predictions in Figure 9 are significantly different as the strain rate increases in the neck. As clearly shown in Figure 9 (right), an abrupt increase in the plastic strain is observed in the neck region, while the plastic strain remains constant far from the neck due to elastic unloading.

The mesh sensitivity of the predicted stress–strain curves was investigated using the elasto-visco-plastic model with Voce hardening. For this material model, a second simulation was performed with an element size twice smaller than the one shown in Figure 8 (*i.e.*, using six

elements through the half-thickness). The two predictions are plotted in Figure 9. Very small mesh sensitivity is only observed by the end of the curves, as the necking phenomenon progresses. These observations corroborate well with the findings of Sung et al. (2010) who successfully predicted the strain-rate influence on the onset of necking on flat steel samples using only two reduced-integration finite elements through the half-thickness, in the framework of von Mises plasticity. A closer recovery of the experimental results would require more refined large strain hardening laws and parameter identification (as strains close to 1 are reached in the neck) and anisotropy (Dunand and Mohr, 2010; Tardif and Kyriakides, 2012). Temperature variation due to the plastic dissipation is also an important factor that can influence the neck geometry evolution and the stress levels. In this context, the aim of the current simulations is simply limited to illustrating the impact of strain-rate sensitivity on the material response even during low speed processes. Figure 10 qualitatively illustrates this result in terms of neck geometry evolution, showing the well-known stabilizing effect of strain-rate sensitivity. It is worth noting that different approaches have been proposed in the literature to reconcile the measured and predicted post-necking responses (Zhang et al., 1999; Kajberg and Lindkvist, 2004; Joun et al., 2008; Mohr and Ebnoether, 2009; Pierron et al., 2010). Note that all of the above-mentioned approaches for the determination of the true stress–strain curve after diffuse necking have been applied to strain-rate independent materials. In the current work, we emphasize the effect of strain-rate sensitivity on the structural force–displacement response of a flat specimen under tension. Another effect that has not been considered in the current analysis is related to the temperature evolution within the sample. Sung et al. (2010) have also used the flat tensile test to illustrate the prominent role of strain rate on the tensile response as soon as necking occurs; temperature had a similarly important role for dynamic tensile tests, while it remained negligible for low nominal strain rates (10^{-3} s^{-1}). The temperature effects were shown to have a determinant role for the prediction of the so-called shear fracture, in particular for HS steels, when little or no necking precedes the fracture (Kim et al., 2011; Sung et al., 2012).

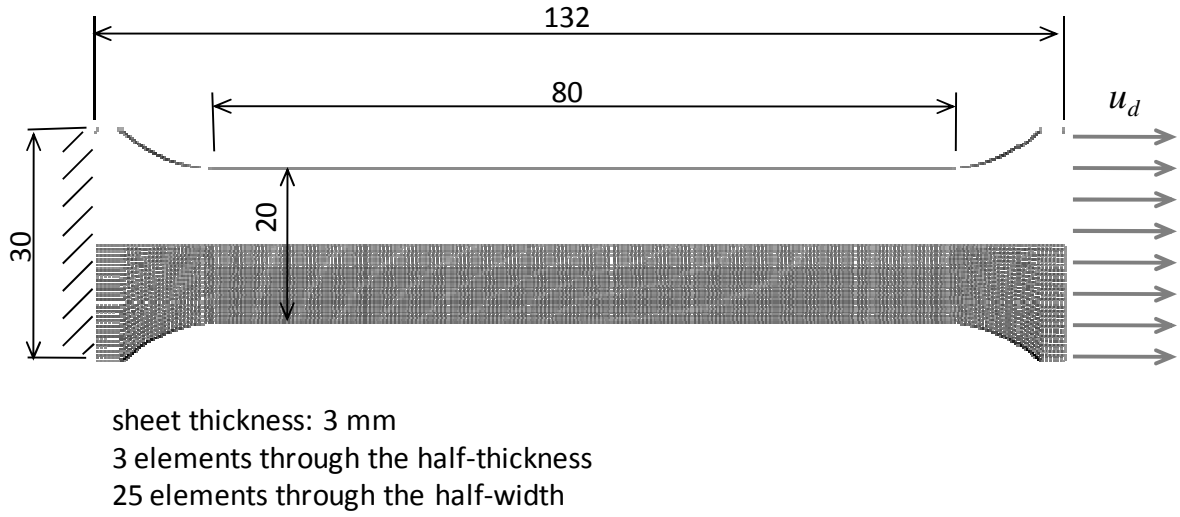

Figure 8. Geometry, loading and mesh used for the finite element simulation of the uniaxial tensile tests.

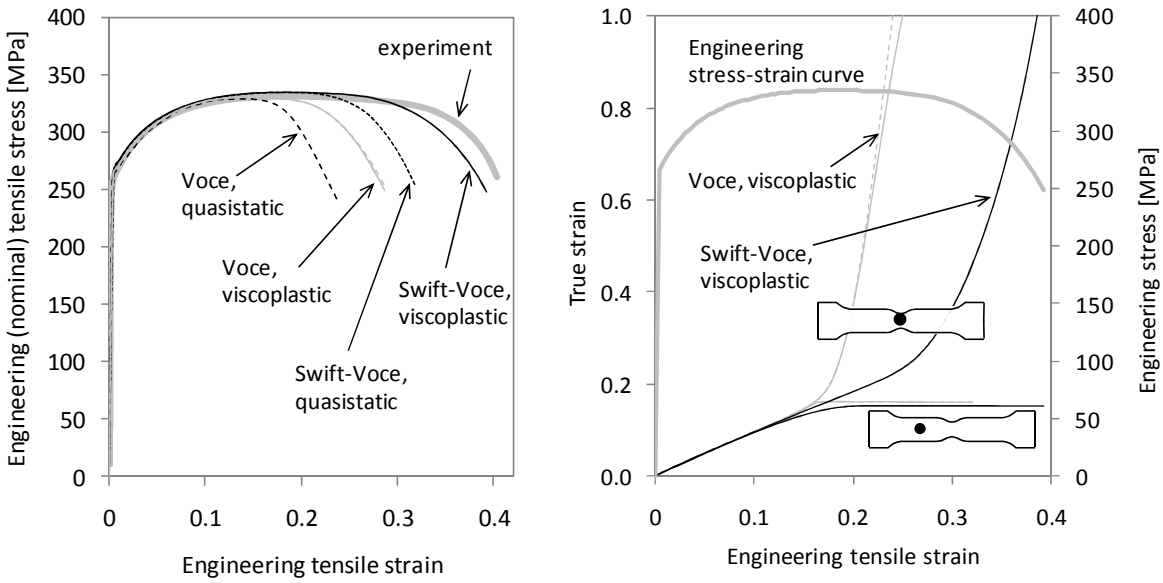

Figure 9. Results of the finite element simulation of the tensile test. Left: predicted and experimental engineering stress–strain curves. Right: longitudinal strain evolution at two material points located in the neck zone and far from the neck. For the "Voce viscoplastic" model, the dashed line corresponds to the finer mesh and the solid line to the coarser mesh.

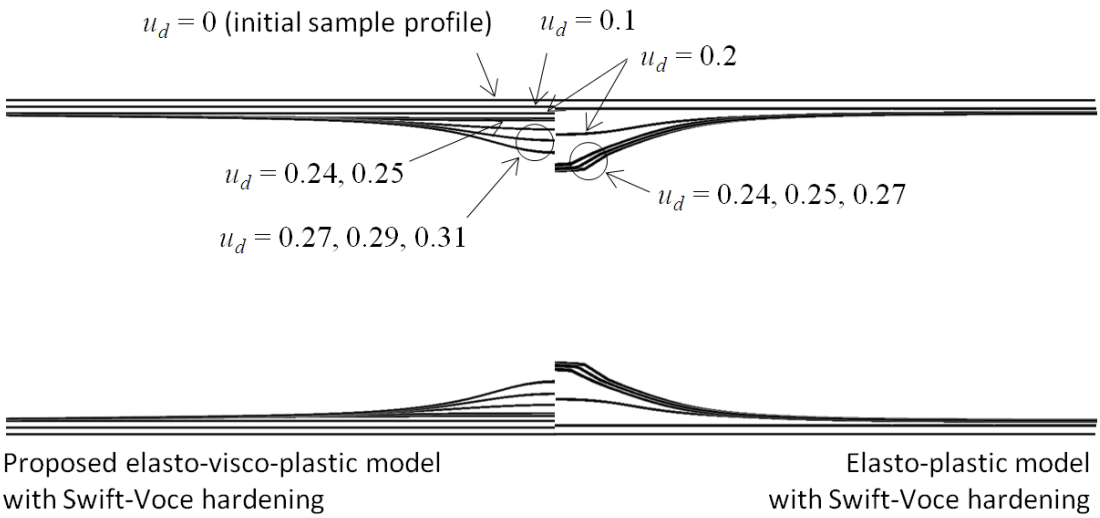

Figure 10. Necking profiles predicted with the S–V elasto-visco-plastic model (left) and the S–V elasto-plastic model (right). The cross-bar displacements corresponding to each profile are indicated.

5 Conclusions

In this work, a new elasto-visco-plastic model has been proposed as a pragmatic alternative to existing state-of-the-art models. One advantage of the proposed model is the reduced number of fitting material parameters, thanks to the physical basis of the adopted constitutive modeling approach. To be specific, only two parameters are required for the strain-rate sensitivity equations, while the available models usually require at least twice as many parameters. In addition, the proposed constitutive framework is independent of the hardening equations. Therefore, the model can be coupled with virtually any anisotropic yield surface or work-hardening model, which is potentially important for future applications where refined descriptions of anisotropy and/or hardening are essential.

The predictive capabilities of the model have been assessed by confrontation to experimental results for three different mild steels, consisting of tensile tests up to strain rates of 10^3 s^{-1}, and quasi-static monotonic and reverse shear tests at different amounts of pre-strain. Also, the model was compared to two recent existing models with respect to experimental results from literature. In spite of the reduced number of material parameters and the simple identification procedure, the model showed reasonably good accuracy in the tested configurations.

Acknowledgments

The authors are grateful to Olivier Bouaziz from ArcelorMittal Research and to Marcel Berveiller from Arts et Métiers ParisTech – Metz for fruitful discussions and guidance. The financial support from ArcelorMittal Research Maizières-lès-Metz and from the Région Lorraine is gratefully acknowledged.

References

Allain, S., Bouaziz, O., Lemoine, X., 2009. A viscoplastic behavior law for ferritic steels at low homologous temperature. Revue de Métallurgie 106 (2), 80–89.

Allain, S., Bouaziz, O., Château, J.P., 2010. Thermally activated dislocation dynamics in austenitic FeMnC steels at low homologous temperature. Scripta Materialia 62, 500–503.

Barlat, F., Gracio, J.J., Lee, M.-G., Rauch, E.F., Vincze, G., 2011. An alternative to kinematic hardening in classical plasticity. Int. J. Plasticity 27, 1309–1327.

Berbenni, S., Favier, V., Lemoine, X., Berveiller, M., 2004. Micromechanical modeling of the elastic-viscoplastic behavior of polycrystalline steels having different microstructures, Materials Science and Engineering A 372, 128–136.

Bouaziz, O., Dirras, G., 2006. Effet de taille de grain sur les écrouissages isotrope et cinématique dans la gamme 0,35 à 75 microns. In : Proc. Matériaux 2006, Dijon, 13–17 November 2006.

Bui-Van, A., Allain, S., Lemoine, X., Bouaziz, O., 2009. An improved physically based behaviour law for ferritic steels and its application to crash modeling. Int. J. Mater. Form. 2, 527–530.

Campbell, J.D., Ferguson, W.G., 1970. The temperature and strain-rate dependence of the shear strength of mild steel. Phil. Mag. 21, 63–82.

Cowper, G.R., Symonds, P.S., 1952. Strain hardening and strain rate effects in the impact loading of cantilever beams. Brown Univ., Div. of Appl. Mech., Report no. 28.

Dunand, M., Mohr, D., 2010. Hybrid experimental-numerical analysis of basic ductile fracture experiments for sheet metals. Int. J. Solids Struct. 47, 1130–1143.

Durrenberger, L., Lemoine, X., Molinari, A., 2011. Effects of pre-strain and bake-hardening on the crash properties of a top-hat section, Journal of Materials Processing Technology 211, 1937– 1947.

Fields, D.S., Bachofen, W.A., 1957. Determination of strain hardening characteristics by torsion testing. ASTM, Proc AM Soc Test Mater 57, 1259–1272.

Geng, L., Shen, Y., Wagoner, R.H., 2002. Anisotropic hardening equations derived from reverse-bend testing. Int. J. Plasticity 18 (5–6), 743–767.

Haddad, A., Balan, T., Abed-Meraim, F., 2003. On the implementation of hardening models in sheet forming simulations. In: Proc. Esaform, April 28-30, Salerno, Italy, 187–190.

Haddadi, H., Bouvier, S., Banu, M., Maier, C., Teodosiu, C., 2006. Towards an accurate description of the anisotropic behaviour of sheet metals under large plastic deformations: Modelling, numerical analysis and identification. Int. J. Plasticity 22 (12), 2226–2271.

Haddag, B., Balan, T., Abed-Meraim, F., 2007. Investigation of advanced strain-path dependent material models for sheet metal forming simulations. Int. J. Plasticity 23, 951–979.

Johnson, G.R., Cook, W.H., 1983. A constitutive model and data for metals subjected to large strains, high strain rates and high temperatures. In: Proc. 7th Int. Symp. on Ballistics, 541–547.

Joun, M.S., Eom, J.G., Lee, M.C., 2008. A new method for acquiring true stress–strain curves over a large range of strains using a tensile test and finite element method. Mech. Mater. 40, 586–593.

Kajberg, J., Lindkvist, G., 2004. Characterisation of materials subjected to large strains by inverse modelling based on in-plane displacement fields. Int. J. Solids Struct. 41, 3439–3459.

Khan, A.S., Huang, S., 1992. Experimental and theoretical study of mechanical behavior of 1100 aluminum in the strain rate range 10^{-5}-10^{4} s^{-1}. Int. J. Plasticity 8, 397–424.

Kim, J.H., Sung, J.I., Piao, K., Wagoner, R.H., 2011. The shear fracture of dual-phase steel. Int. J. Plasticity 27, 1658–1676.

Kocks, U.F., Argon, A.S., Ashby, M.F., 1975. Thermodynamics and kinetics of slip. Prog. Mat. Sci. 19, 1–291.

Lemoine, X., 2007. Behavior laws and their influences on numerical prediction. AIP Conf. Proc. 907, 269–274.

Lemoine, X., Sriram, S., Kergen, R., 2011. Flow curve determination at large plastic strain levels to accurately constitutive equations of AHSS in forming simulation. AIP Conf. Proc. 1353, 1417–1422.

Liang, R., Khan, A.S., 1999. A critical review of experimental results and constitutive models for BCC and FCC metals over a wide range of strain rates and temperatures. Int. J. Plasticity 15, 963–980.

Mohr, D., Ebnoether, F., 2009. Plasticity and fracture of martensitic boron steel under plane stress conditions. Int. J. Solids Struct. 46, 3535–3547.

Molinari, A., Canova, G.R., Ahzi, S., 1987. A self consistent approach of the large deformation polycrystal viscoplasticity. Acta Metallurgica 35, 2983–2994.

Molinari, A., Ravichandran, G., 2005. Constitutive modeling of high-strain-rate deformation in metals based on the evolution of an effective microstructural length. Mech. Mater. 37, 737–752.

Perzyna, P., 1963. The constitutive equations for rate sensitive plastic materials. Quart. Appl. Math. 20, 321–332.

Pierron, F., Avril, S., The Tran, V., 2010. Extension of the virtual fields method to elasto-plastic material identification with cyclic loads and kinematic hardening. Int. J. Solids Struct. 47, 2993–3010.

Pilvin, P., 1990. Approches multiéchelles pour la prévision du comportement anélastique des métaux. PhD thesis, Université Paris 6, Paris, France.

Pipard, J.M., 2012. Modélisation du comportement élasto-viscoplastique des aciers multiphasés pour la simulation de leur mise en forme. PhD thesis, Arts et Métiers ParisTech, Metz, France.

Preston, D.L., Tonks, D.L., Wallace, D.C., 2003. Model of plastic deformation for extreme loading conditions, J. Appl. Phys. 93, 211–220.

Rauch, E.F., 1994. Relation between forest dislocations and stress in bcc metals. Key Eng. Mater. 97-98, 371–376.

Rusinek, A., Klepaczko, J.R., 2001. Shear testing of a sheet steel at wide range of strain rates and a constitutive relation with strain-rate and temperature dependence of the flow stress. Int. J. Plasticity 17, 87–115.

Rusinek, A., Zaera, R., Klepaczko, J.R., 2007. Constitutive relations in 3-D for a wide range of strain rates and temperatures – Application to mild steels. Int. J. Solids Struct. 44, 5611–5634.

Sabar, H., Berveiller, M., Favier, V., Berbenni, S., 2002. A new class of micro-macro models for elastic-viscoplastic heterogeneous materials. Int. J. Solids Struct. 39, 3257–3276.

Seeger, A., 1955. The generation of lattice defects by moving dislocations, and its application to the temperature dependence of the flow-stress of F.C.C. crystals. Phil. Mag. 46, 1194.

Sellars, C.M., Tegart, W.J.M., 1966. La relation entre la résistance et la structure dans la déformation à chaud. Mem. Sci. Rev. Met. 63, 731–746.

Sung, J.I., Kim, J.H., Wagoner, R.H., 2010. A plastic constitutive equation incorporating strain, strain-rate, and temperature. Int. J. Plasticity 26, 1746–1771.

Sung, J.I., Kim, J.H., Wagoner, R.H., 2012. The draw-bend fracture test and its application to dual-phase and transformation induced plasticity steels. J. Eng. Mater. Techn. 134, 041015.

Tardif, N., Kyriakides, S., 2012. Determination of anisotropy and material hardening for aluminum sheet metal. Int. J. Solids Struct. 49, 3496–3506.

Tarigopula, V., Hopperstad, O.S., Langseth, M., Clausen, A.H., Hild, F., A study of localisation in dual-phase high-strength steels under dynamic loading using digital image correlation and FE analysis. Int. J. Solids Struct. 45, 601–619.

Teodosiu, C., Hu, Z., 1995. Evolution of the intragranular microstructure at moderate and large strains: modelling and computational significance. In: Shen, S., Dawson, P.R. (Eds.), Proc. Numiform'95, Balkema, Rotterdam, 173–182.

Teodosiu, C. (Ed.), 1997. Large Plastic Deformation of crystalline aggregates. CISM courses and lectures – No. 376, ISBN: 3-211–82909.

Uenishi, A., Teodosiu, C., 2003. Solid solution softening at high strain rates in Si- and/or Mn-added interstitial free steels. Acta Materialia 51, 4437–4446.

Uenishi, A., Teodosiu, C., 2004. Constitutive modelling of the high strain rate behaviour of interstitial-free steel. Int. J. Plasticity 20, 915–936.

Uenishi, A., Teodosiu, C., Nesterova, E.V., 2005. Microstructural evolution at high strain rates in solution-hardened interstitial free steels. Mat. Sci. Eng. A 400–401, 499–503.

Wong, W.A., Jonas, J.J., 1968. Aluminium extrusion as a thermally activated process. Trans. AIME 242, 2271–2280.

Yoshida, F., Uemori, T., 2002. A model of large-strain cyclic plasticity describing the Bauschinger effect and work hardening stagnation. Int. J. Plasticity 18, 661–686.

Zerilli, F.J., Armstrong, R.W., 1987. Dislocation-mechanics-based constitutive relations for material dynamics calculations. J. Appl. Phys. 61, 1816–1825.

Zhang, H.J., Wen, W.D., Cui, H.T., Xu, Y., 2009. A modified Zerilli-Armstrong model for alloy IC10 over a wide range of temperatures and strain rates. Mat. Sci. Eng. A 526, 1–6.

Zhang, Z.L., Hauge, M., Odegard, J., Thaulow, C., 1999. Determining true stress–strain curve from tensile specimens with rectangular cross-section. Int. J. Solids Struct. 36, 3497–3516.

Zhao, H., Gary, G., 1996. The testing and behaviour modelling of sheet metals at strain rates from 10^{-4} to 10^{4} s^{-1}. Mater. Sci. Eng. A 207, 46–50.